INTERNATIONAL JOURNAL OF CLIMATOLOGY
Int. J. Climatol. (2014)
Published online in Wiley Online Library
(wileyonlinelibrary.com) DOI: 10.1002/joc.4185

RMetS
Royal Meteorological Society

Variability in the annual cycle of the Río Atuel streamflows and its relationship with tropospheric circulation

Diego Araneo[a,b]* and Ricardo Villalba[a]

[a] *Instituto Argentino de Nivología, Glaciología y Ciencias Ambientales (IANIGLA), CONICET-CCT-Mendoza, Argentina*
[b] *Instituto de Ciencias Básicas (ICB), Universidad Nacional de Cuyo, Mendoza, Argentina*

ABSTRACT: Climate-induced changes in the annual regime of snow-fed rivers have serious implications for water resource management. In the Central Andes (CA, 28°–36°S) of Argentina–Chile, the snow accumulated in high-elevation mountains in winter is the dominant component of streamflows during the spring–summer melting season. Although topography introduces complexity in snowpack responses to the annual temperature cycle, streamflow series over a century in length make the CA particularly suitable for identification of long-term hydrological changes. Principal component (PC) analysis of Río Atuel annual hydrographs from 1906 to 2012 discriminates between precipitation- and temperature-related components associated with variations in snow accumulation (49% of variance) and advances/delays of the streamflow annual peak (21% of variance), respectively. The temporal evolution of PC1 loadings reveals a predominant negative period from 1917 to 1976 and from 1988 to present, suggesting the propensity to undergo long periods with reduced flows. In turn, the PC2 pattern is predominantly positive from 1948 to the present, revealing a tendency to more frequent peak flows in late spring since the mid-20th century. Above-average streamflows related to abundant snowfalls in the CA are associated with northward shifts in stormtracks that are remotely induced by above-average sea surface temperatures in the equatorial Pacific. On the other hand, earlier streamflow peaks in November-December are concurrent with above-average temperatures across the Atuel basin induced by enhanced meridional circulation from the Tropics due to the strengthening of the South Atlantic anticyclone. These circulation anomalies are linked to the persistent positive phase of the Southern Annular Mode during the last decades. Additionally, years with reduced streamflows in January, and proportionally larger flow contributions in November-December, are associated with anomalous air cooling at high levels induced by low pressure centres over the region as part of a quasi-zonal stationary Rossby wave train that extends from Australia to the South American–South Atlantic sector.

KEY WORDS Río Atuel; streamflows annual cycle; tropospheric circulation; principal component analysis; El Niño; Southern Annular Mode; Rossby waves

Received 17 December 2013; Revised 19 August 2014; Accepted 15 September 2014

1. Introduction

Changes in the amount and timing of water released from the snowpack in the high mountains are issues of social and environmental concerns. The Central Andes (CA) of Argentina and Chile (28°–36°S) are characterized by an arid to semi-arid climate where most streamflow originates from the snowpack in the mountains (Masiokas *et al.*, 2006). The snowpack represents a natural reservoir of water, released primarily during the spring and summer, and constitutes the key driver of socio-economic activities on both sides of the Andes. Most runoff from snowpack is used for irrigation. In addition, snowmelt-derived runoff is the major source of water for human consumption, industrial activities and regional hydropower generation.

Recent studies in the western United States have documented a significant reduction in snow water equivalent and an advance in the timing of runoff resulting from melting snow (Mote *et al.*, 2005; Pierce *et al.*, 2008). These changes have been accompanied by a higher proportion of rain *versus* snow in total precipitation and a significant increase in winter flows as a percentage of the annual total flows. These hydrological changes have been generally associated with increases in minimum temperatures during winter and spring, generally related to global warming processes (Dettinger *et al.*, 2004; Knowles and Cayan, 2004; Regonda *et al.*, 2005, Stewart *et al.*, 2005; Hamlet *et al.*, 2007; Barnett *et al.*, 2008; Clow, 2010). At local or regional scales, the observed changes in hydrology are more complex and involve interactions between topography and atmospheric circulation from synoptic to hemispheric scales. For example, in the western United States, interannual to decadal variations in hydrology are strongly influenced by atmosphere–ocean interactions involving components of both the tropical and North Pacific Oceans (Cayan *et al.*, 1998).

The Cordillera de los Andes in Argentina ranges from subtropical (22°S) to sub-Antarctic (54°S) latitudes. The climate along this long mountainous range is extremely diverse changing from mild and dry in the northern subtropics to cold and wet in the southern temperate

* Correspondence to: D. C. Araneo, Instituto Argentino de Nivología, Glaciología y Ciencias Ambientales (IANIGLA), CONICET-CCT-Mendoza, Av. Ruiz Leal s/n., Parque Gral. San Martín, CC 330, 5500 Mendoza, Argentina. E-mail: daraneo@mendoza-conicet.gob.ar

regions. With a mean elevation of about 5000 m, the CA (28°–36°S) form a permanent barrier to the ingression of moisture from the Pacific Ocean resulting in desert and or semi desert conditions east of the main Cordillera with total annual rainfalls about 200 mm (Prohaska, 1976, Schwerdtfeger, 1976). At high elevations in the CA, winter precipitation commonly occurs as snow. Snow melting starts at lower elevations in September, reaches the high mountains (above 4500 m) in late October–November and peaks in December–January.

Although most of the annual discharge occurs during the warm, snowmelt dominated spring–summer period of the year, the total amount of water depends primarily on the snow accumulated during the previous winter on the high-elevation mountains. Consequently, interannual variations in precipitation and therefore in snowmelt runoff volumes are controlled by the atmospheric circulation during the cold period of the year. Hoffman (1969) showed that snow accumulation on the higher mountains, and consequently total streamflows on both sides of the CA, is closely related to rainfall variations in Central Chile, which occurs almost entirely during winter months (see also Masiokas *et al.*, 2012). The interannual variability of runoff in the CA has been associated with the El Niño-Southern Oscillation (ENSO), showing a tendency for exceptionally heavy snowfalls in the CA during El Niño years (Pittock, 1980; Quinn and Neal, 1983). Aceituno (1988) showed that abnormally heavy rainfalls in Central Chile, during the negative phase of the Southern Oscillation, are related to the weakening and northward shift of the South Pacific subtropical anticyclone in winter. In addition, Ruttlant (1987), and Ruttlant and Fuenzalida (1991), attributed the abundant winter precipitation in Central Chile during El Niño events to more frequent and persistent blocking ridges in the westerly flow southwest of South America (SA). These blocking episodes form part of a wave train structure, particularly intense during the spring, characterized by a sequence of positive and negative anomaly centres of geopotential height (HGP) with a quasi-barotropic structure that extends from tropical to southeast Pacific and reaches the southwest Atlantic Ocean (Montecinos and Aceituno, 2003).

Consistent with these observations, above normal runoff in the CA has been associated with positive sea-surface temperature (SST) anomalies in the equatorial Pacific (Aceituno and Vidal, 1990; Waylen and Caviedes, 1990; Masiokas *et al.*, 2006). Escobar and Aceituno (1998) showed the influence of SST extremes on precipitation in the Andean sector of Chile, with abundant or reduced snow accumulation for El Niño and La Niña events, respectively. Consequently, the warm and cold phases of ENSO are respectively related to above- and below-average streamflows in the CA of Chile (Aceituno and Garreaud, 1995) and Argentina (Compagnucci and Vargas, 1998). More recently, Compagnucci and Araneo (2007) showed the potential of tropical SST values as predictor of the Argentinean river discharges in the CA based on correlations between peak seasonal discharges and SSTs in the El Niño 3.4 region. These authors showed that correlation coefficients between El Niño 3.4 SST and the river discharges reach the highest r values when SST precedes runoff by 14 and 8 months, respectively for rivers in the northern and southern sectors of the CA in Argentina. Araneo and Compagnucci (2008) noted that high (low) river discharges are related to the weakening (strengthening) of the basic low-level atmospheric circulation. At high levels, a wave pattern in NW–SE direction extending from Australia to the South Atlantic favours the occurrence of positive (negative) pressure anomalies west of the Drake Passage. Consequently, the storm track is deflected northward (southward) increasing (decreasing) precipitation and the subsequent river discharges. Recent analysis by Masiokas *et al.* (2010) and Villalba *et al.* (2012) have also identified possible influences of the Pacific Decadal Oscillation (PDO) and the Southern Annular Mode (SAM; Thompson and Wallace, 2000) in the low-frequency modes of variability in streamflows in the CA and northern Patagonia of Argentina and Chile.

These previous studies have provided a basic picture of the atmospheric circulation features related to the interannual variability of the river regimes in the CA of Argentina and Chile. On the other hand, climatic records in the CA have documented an increase in temperature during the last decades, particularly at high elevations in the Cordillera (+0.25°C/decade since 1979; Carrasco *et al.*, 2005; Falvey and Garreaud, 2009). In this context, it is interesting to analyse potential changes or time displacement in the annual runoff pattern of rivers in the CA. Shifts in the water cycle will introduce variations in water supply over the year with serious implications for water management and meeting the differences in seasonal demand imposed by users (e.g. irrigation *vs* hydropower generation). Although, several studies conducted in diverse mountain regions of the world have documented earlier timing of snowmelt peaks, similar studies in the CA are rare. In a recent analysis of hydrological cycles from several rivers flowing down the Chilean slope of the CA (30°–40°S), Cortés *et al.* (2011) showed a significant shift towards earlier dates of the centre of timing for 23 of the 40 rivers in the region. Although the centre of timing was significantly correlated with air temperature over the period 1961–2006, they recorded no significant change in the centre of timing for most watersheds after 1976, coincident with a marked warming in the region. Indeed, in order of importance, the centre of timing of the hydrological cycle of the rivers on the western slope of the CA showed higher correlation with total annual precipitation, ENSO and, in the third place, with mean winter and spring temperature (Cortés *et al.*, 2011). As no related studies have been conducted on the Argentinean slopes of the CA, it is relevant to characterize past variations in the water cycle and their relationships with large-scale circulation patterns around SA.

In this study, we analyse the interannual variations of Rio Atuel hydrological cycle from 1906 to present. The Rio Atuel runoff is representative of the hydrological regimes on the eastern slope of the CA (Figure 1; Compagnucci and Araneo, 2005). The major modes of variability in the hydrological cycle are identified and their

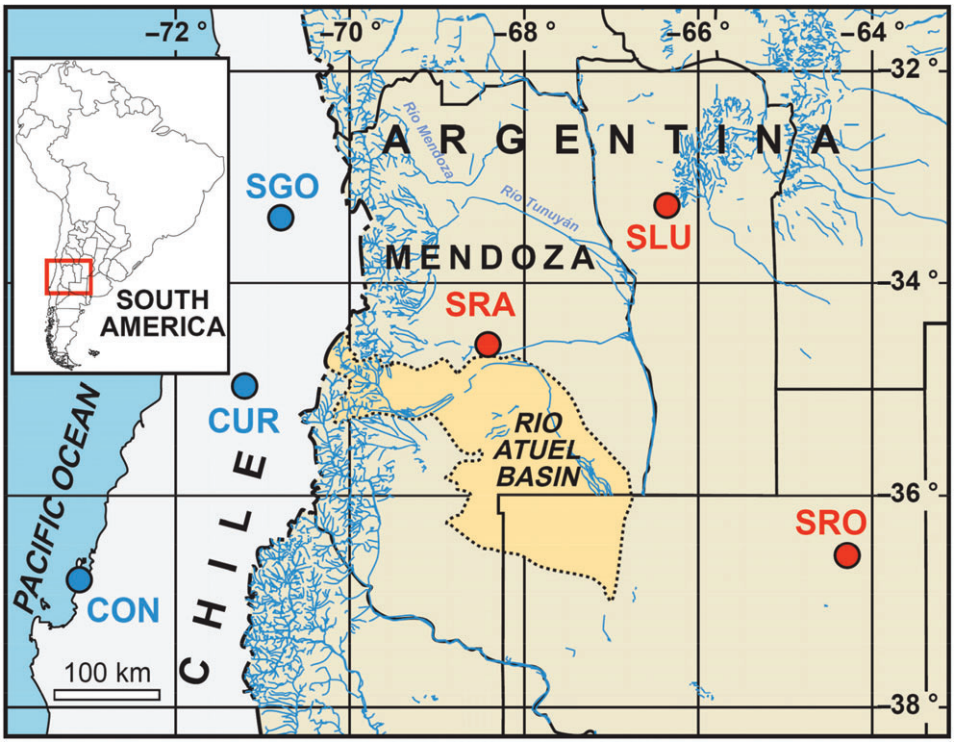

Figure 1. Map of central-western Argentina and central Chile, showing the location of Río Atuel basin and the temperature (red circles in online) and precipitation (blue circles in online) stations used in this study. The international boundary between Chile and Argentina runs mainly along the drainage divide in the Andes.

relationships to regional–hemispheric atmospheric circulation are established. This analysis will provide valuable insights on future changes of the hydrological cycles of Argentinean rivers in the CA, information required to establish mitigation actions intended to reduce impacts on regional economies.

2. Data and methodology

Interannual streamflow variations for most rivers in the CA are highly correlated with each other (Minetti and Sierra, 1989; Compagnucci and Vargas, 1998; Masiokas *et al.*, 2006, 2012). Based on a comparison of temporal variations in streamflow at a regional scale, Compagnucci and Araneo (2005) showed that the monthly runoff variability in the Río Atuel basin is representative of most rivers in the region (mean streamflow correlation coefficient between Atuel and other major rivers in the region is greater than 0.7). Consequently, the temporal variability in CA streamflows is well captured by changes recorded in the Río Atuel discharge.

Monthly streamflow records from Río Atuel at La Angostura gauging station (35°05′57″S; 68°52′26″W; 1200 m) from July 1906 to June 2012 were provided by the Argentinean Water Resource Administration (http://www.hidricosargentina.gov.ar/index.php). The basin area upstream of this gauging station is about 3800 km^2, and there are no human activities in this area that alter the natural runoff (see Figure 1 and Table 1). As Río Atuel shows the maximum and minimum streamflows in summer and winter respectively, we defined the annual flow period as July–June. In order to determine the main characteristics of the interannual variability in the annual hydrological cycle, we applied principal component analysis (PCA) to the 106 complete cycles in the data record. Monthly streamflows were arranged in a matrix $\mathbf{X}_{[12,106]}$ whose columns consist of each annual cycle from 1906 to 2012 arranged from July (year t) to June (year $t+1$). As we were interested in the interannual variability of the annual cycle, the mean monthly values were converted to indices by subtracting the monthly mean for the 106-year record obtaining the deviation matrix $\widetilde{\mathbf{X}}_{[12,106]}$. Based on the deviation matrix, the matrixes of Component Scores $\mathbf{Z}$ (patterns or PCs) and Component Loadings $\mathbf{F}$ (time series of correlation coefficients between patterns and the original variables) were derived as follows:

$$\mathbf{Z} = \widetilde{\mathbf{X}}_{\mathbf{s}}\mathbf{U}$$

$$\mathbf{F} = \mathbf{U}\mathbf{D}^{1/2}$$

where $\widetilde{\mathbf{X}}_{\mathbf{s}}$ is the standardized matrix associated with $\widetilde{\mathbf{X}}$ (i.e. the matrix obtained by subtracting from each element of $\widetilde{\mathbf{X}}$ the average of the corresponding column and dividing that difference by the standard deviation of the corresponding column), and $\mathbf{Q}_{[106\times106]}$ and $\mathbf{D}_{[106\times106]}$ are respectively the matrices of eigenvectors and eigenvalues associated with $\mathbf{R} = \left(\widetilde{\mathbf{X}}_{\mathbf{s}}'\widetilde{\mathbf{X}}_{\mathbf{s}}\right)/12$ (the correlation matrix between columns of $\widetilde{\mathbf{X}}$, and where the prime denotes the transpose of a matrix). Long-term shifts in mean conditions in

Table 1. Meteorological and hydrological data used in this study.

Station name	Latitude	Longitude	Elevation [m]	Variable	Record period	Missing data [%]
Santiago (SGO)	33.38°S	70.78°W	520	PP	1867–2010	6.77
Curicó (CUR)	34.97°S	71.20°W	225	PP	1951–2010	32.64
Concepción (CON)	36.80°S	73.10°W	11	PP	1912–2010	0.76
San Luis (SLU)	33.27°S	66.35°W	713	T	1931–2010	0.73
San Rafael (SRA)	34.58°S	68.40°W	748	T	1961–2010	3.17
Santa Rosa (SRO)	36.57°S	64.27°W	191	T	1941–2010	6.43
La Angostura	35.10°S	68.87°W	1200	SF	1906–2012	0.00

PP, precipitation; T, temperature; SF, streamflow.

the time series of the PC loadings (PCLs) were identified using a simple regime shift detection technique (Rodionov, 2004) with a cut-off segment length $l = 20$ years, a target probability level $p = 0.2$, and an outlier weighting factor $h = 1$.

In order to determine the relationships between local and global atmospheric–oceanic features and the variability in the streamflow annual cycle, the following variables were considered: monthly HGP (in mgp), wind vector (V, in $\mathrm{m\,s^{-1}}$), precipitable water (PW, in mm) and temperature (T, in °C) at 925, 700 and 500 hPa levels in a global regular 2.5° × 2.5° latitude–longitude grid. In addition, velocity potential (Chi, in $\mathrm{m^2\,s^{-1}}$) and streamfunction (Psi, in $\mathrm{m^2\,s^{-1}}$) at $\sigma = 0.995$, 0.846, 0.258 and 0.168, in a global T62 Gaussian grid (192 × 94) were also investigated. All these data were obtained from the NCEP Reanalysis 1 dataset (period 1948–2012; see Kalnay *et al.*, 1996). The Extended Reconstructed Sea-Surface Temperature (ERSST-V3) from NOAA's Physical Sciences Division (period 1854–2012, with ocean coverage of 2.0° × 2.0° latitude–longitude grid) and the University of Delaware surface temperature and precipitation data (V3.01, period 1901–2010, with land coverage of 0.5° × 0.5° latitude–longitude grid) were provided by the NOAA/OAR/ESRL PSD website at http://www.esrl.noaa.gov/psd/. Precipitation data from Santiago (SGO), Curicó (CUR) and Concepción (CON), and temperature records from San Luis (SLU), San Rafael (SRA) and Santa Rosa (SRO) stations (see Figure 1 and Table 1) were used as regional control. These meteorological records were provided by the National Weather Services of Chile and Argentina.

Spatial correlation fields between PCL time-series (columns of **F**) and meteorological–oceanic variables were estimated for each month over the period 1958–2011. Correlations with the wind vector were calculated separately for the zonal (r_u) and meridional (r_v) wind components. Correlation coefficient significances at 90, 95, 99 and 99.5% confidence levels were determined using the Student *t*-test. The $\vec{\mathbf{r}} = r_u\hat{\mathbf{i}} + r_v\hat{\mathbf{j}}$ vectors were considered significant when at least one of their components (r_u or r_v) is higher than the critical value at the 95% significance level. Finally, spatial composite fields of meteorological–oceanic variables were developed for years or long-term periods with persistent positive and negative PCLs. Spatial composite anomaly significances at 90 and 95% confidence levels were also determined using the Student *t*-test.

3. Results

3.1. Patterns of Río Atuel streamflows annual cycle

The average annual cycle of Río Atuel monthly runoff shows the maximum and minimum streamflows in January and June, respectively (Figure 2). For Río Atuel, the interseasonal mean difference between summer (DJF) and winter (JJA) is about $37\,\mathrm{m^3\,s^{-1}}$, representing 170% increase between mean winter and summer flows. According to the PCA, the first two PCs explained more than 70% of the total variance in the annual cycles of Río Atuel streamflows. PC1 explains 49.3% of the total variance and accounts for the variations in the streamflow annual cycle associated with above-average (+Z1) or below-average (−Z1) discharges in relation to the mean cycle (Figure 2, Z1). This component represents a runoff excess or deficit

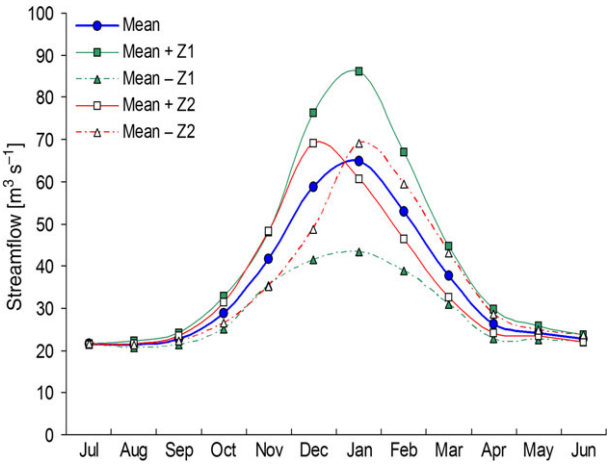

Figure 2. The mean annual hydrological cycle of Río Atuel (blue line with dots in online) and its more frequent deviations estimated from a PCA of the annual cycle over the interval 1906–2012. The interannual variability of Río Atuel annual cycle can be decomposed into a snow-dependent component, related to the above (Mean + Z1)/below (Mean − Z1) normal runoff variability (PC1) and into a thermal-dependent component of spring–summer, which determines the seasonal shift (early peak: Mean + Z2/late peak: Mean − Z2) of the monthly streamflow peak (PC2). As the Z components are non-dimensional, the scale in the *y*-axis (in $\mathrm{m^3\,s^{-1}}$) is valid for the mean hydrograph and illustrative for the PC patterns.

during the warm season compared with long-term average values. Consequently, the first component is strongly related to the total annual discharge and its interannual variability, because most of the annual runoff volume corresponds to the period from November to March (warm season). The second component (Figure 2, Z2) explains 21.1% of the total variance and is associated with an advance (to late spring and early summer; +Z2) or a delay (to late summer; −Z2) of the annual streamflow peak.

As the PCLs are the correlation coefficients between the annual cycles of each year and the main PC patterns described above, positive and negative loadings are related directly or inversely, respectively, to the corresponding PC. PC1 is associated with excess or deficit in the annual streamflow; therefore, the corresponding PC1 loadings (PC1Ls) (Figure 3(a)) are highly correlated with total annual runoff (correlation coefficient $r = 0.80$, $n = 106$). The accumulated PC1Ls mainly increase from 1906 to 1916 and from 1977 to 1987 and decrease from 1917 to 1976 and from 1988 to 2011, consistent with periods dominated by positive (years of abundant discharge) and negative (years of reduced discharge) PC1L values, respectively. Mean PC1Ls, averaged for those mostly positive *vs* negative periods are significantly different at the 1% level according to the Student *t*-test, and therefore the years 1916–1917, 1976–1977 and 1987–1988 represent times of hydrological discontinuities, which are also detected by the Rodionov's (2004) regime shift detection method. The mean annual hydrological cycle for the mostly positive PClL years shows a mean streamflow greater than the mean for the mostly negative PClL years in all months (Figure 3(c)), reflecting differences induced by interannual and long-term variability. The greatest difference is observed in January ($24\ m^3\ s^{-1}$), and the mean cumulative annual volume for the negative PCl periods represents a reduction of 23% with respect to that corresponding to the positive PCl periods.

The accumulated PCLs time series corresponding to PC2 (Figure 3(b)) shows a predominant decreasing trend from 1906 to 1926, is constant from 1927 to 1947 and shows an increasing trend from 1948 to 2011. Consequently, PC2 loadings (PC2Ls) are mostly negative for the first period and positive for the third, while the second interval shows both positive and negative values. The mean values of PC2Ls, averaged over the first and third periods are significantly different at 0.5% level according to the Student *t*-test. This represents a change in the annual streamflow regime that includes two jumps or discontinuities in the years 1926–1927 and 1947–1948, also detected by the Rodionov's (2004) method. Figure 3(d) shows annual hydrological cycles averaged for the three periods. The transition from mostly negative PC2 in the period 1906–1926 to positive PC2Ls in the period 1948–2011 is associated with the advance and larger contribution of November and December streamflows followed by the reduction of January to April streamflow contribution to the annual discharge. The differences in monthly contribution to Río Atuel streamflow between the first and third periods correspond to a mean increase in November runoff of about $+7\ m^3\ s^{-1}$ and a mean decrease in February runoff of about $-15\ m^3\ s^{-1}$. Based on the long-term mean (1906–2011) monthly discharges, these changes represent an increase of 17% in November and a reduction of 28% in February streamflows. Comparing the second and third periods, a slight streamflow increase is recorded in November and December.

3.2. Atmospheric–oceanic circulation associated with the Río Atuel annual cycle variations

The comparison of the PCLs from PC1 and PC2 with several meteorological fields provides a degree of association between the large-scale atmospheric circulation and variations in the annual streamflow cycle. As positive (negative) values in the field are associated with direct (inverse) relationships between climate variables and the PCLs, direct (opposite) signs in the fields correspond to climate anomalies associated with the PC patterns in direct + Z (inverse −Z) modes.

3.2.1. Circulation patterns associated with PC1

The most consistent spatial correlation patterns between PC1 and climate are recorded over the June–November period. Although PC1 represents excess or deficit in late spring–summer (November–March) streamflows, these variations are related to previous winter and spring (June–November) snow precipitation. Figure 4 (left panels) shows the corresponding correlation fields between PC1Ls and HGPs and wind vectors (V) at 500 (a) and 925 hPa (b). At low levels, positive correlations occur over the Drake Passage in the southern Pacific. For above-average discharges in Río Atuel, wind correlation vectors exhibit a circulation associated with a high-pressure centre on the Drake region concurrent with a strong reduction of the Westerlies between 40° and 60°S across Patagonia. Negative correlations crossing the continent at mid latitudes indicate a large number of low-pressure systems from the Pacific crossing the Andes during years with abundant runoff. In contrast, the strengthening of the semi-permanent Pacific and Atlantic anticyclones are related to dry events. At high levels, positive significant correlations over the Amundsen-Bellingshausen Seas are shifted westward with respect to surface anomalies (about 8° longitude between 500 and 1000 hPa) suggesting more frequent passage of dynamic systems at these latitudes. The area with negative values at mid-latitudes splits into two centres located east and west of the Andes with a relative anticyclonic circulation between both centres, E of the Andes. Over the Río Atuel basin, NW airflows from the subtropical Pacific are associated with runoff excesses (vice versa for deficits). In the central Pacific, the negative correlation centre over 130°W–40°S at 925 hPa is displaced 10° westward at 500 hPa, an indication of an increase in the number of baroclinic transient systems in this region. This centre is part of a quasi-stationary wave train crossing the Pacific in NW–SE direction from a positive centre over Southern Australia to a negative one over the South Atlantic Ocean. This wave train

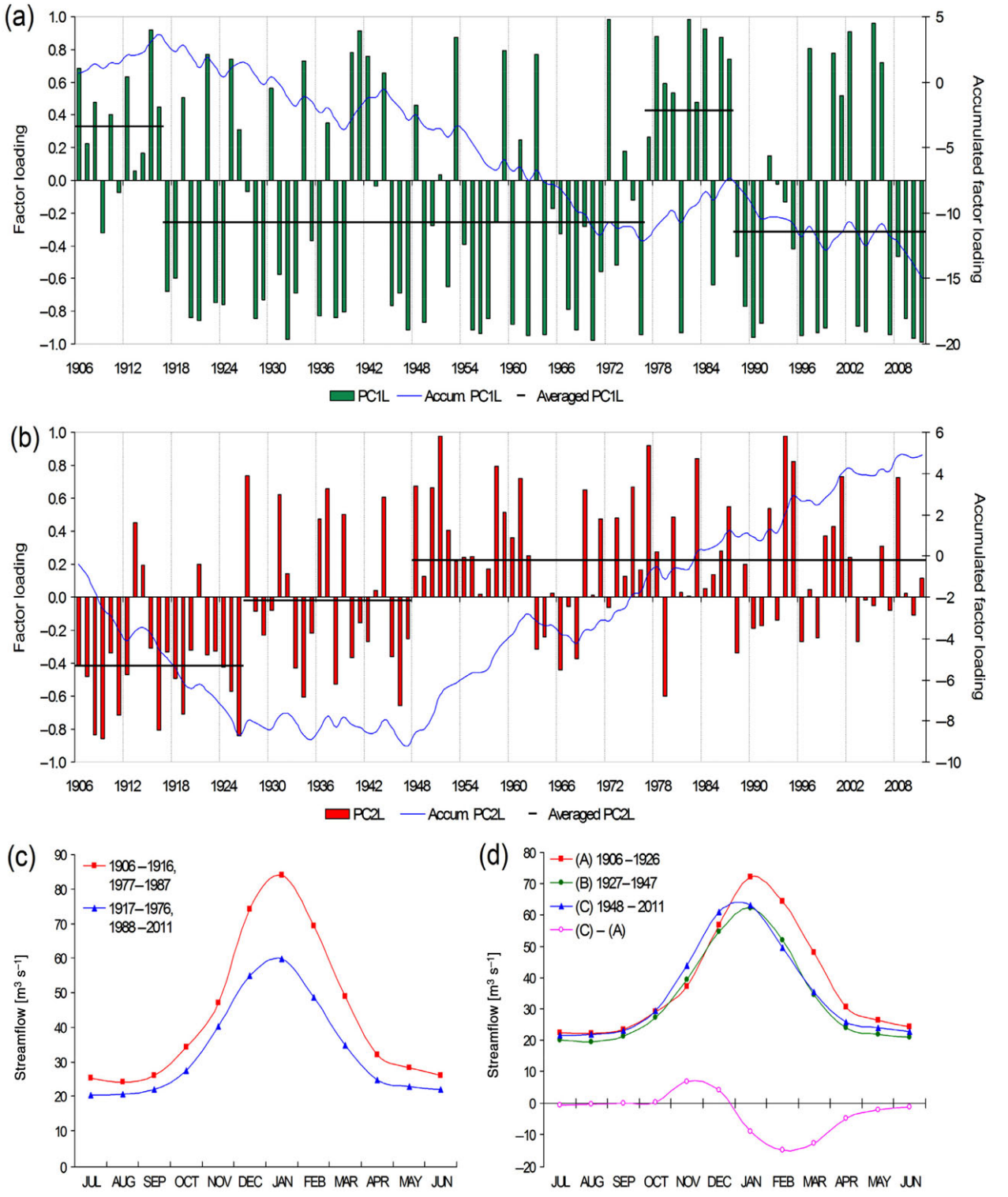

Figure 3. PC1 (a) and PC2 (b) loadings and their respective accumulated values (thin lines). Thick lines indicate mean values for each period. Mean hydrographs associated with PC1Ls and PC2Ls for particular periods are shown in panels (c) and (d), respectively. In panel (d), the wavy line at the bottom shows differences in mean hydrographs between the periods 1948–2011 and 1906–1926.

resembles the second Pacific–South American (PSA2) leading pattern of circulation variability in the Southern Hemisphere identified by Mo (2000) and associated with the quasi-biennial (26 months) component of ENSO variability. The presence of positive and negative centres, respectively at 35° and 40°S over the South American continent at 500 hPa, increases high-level winds over the Río Atuel basin.

The correlation fields between PC1Ls and the stream-function (Psi) at $\sigma = 0.99$ and 0.26 levels, together with those for PW, are shown in Figure 4 (right panels). To facilitate the interpretation, vectors representing the

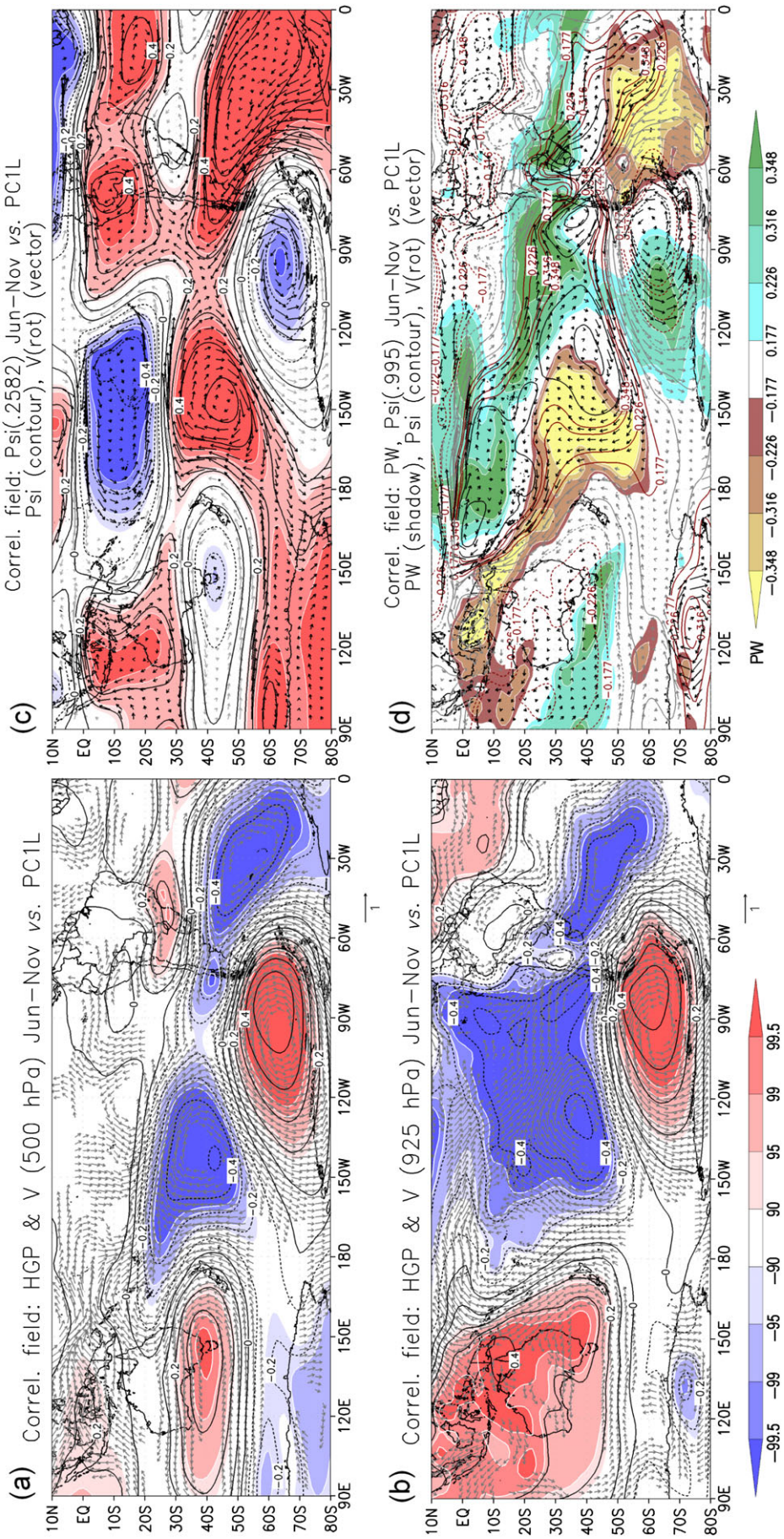

Figure 4. Correlation fields between PC1L and atmospheric circulation variables. Left panels: Correlation fields between PC1L and June–November average for wind and geopotential height at 500 (a) and 925 hPa (b). Shaded areas, from light to dark, correspond to significant values at 90, 95, 99 and 99.5% levels (positive in red and negative in blue in online). For wind correlation vectors, only those with at least one significant component – u or v – at the 95% level are included. Right panels: as in left panels but for streamfunction at $\sigma = 0.2582$ (c) and for streamfunction at $\sigma = 0.995$ and precipitable water (d). In panel (d), the significant values at 90, 95, 99 and 99.5% levels are indicated by shaded areas for the precipitable water and by lines (red in online) for the streamfunction. In both panels (c) and (d), vectors represent the non-divergent circulations associated with the correlations with the streamfunction (in grey for non-significant ones).

non-divergent wind fields are also shown. At low levels, positive centres are displayed over the southern South American coast associated with the HGP anomalies at the same locations. Positive correlations with the PW and non-divergent wind component at low levels in NW–SE direction from the Pacific are consistent with increased moisture advection over Río Atuel basin. Over the tropical Pacific (~10°S–160°W), the rotational wind component reveals the occurrence of cyclonic and anticyclonic circulations at the surface and at high levels, respectively, linked to the presence of anomalous warm low (or cold high) pressures over the region. Also related to that circulation, anomalous western and eastern air fluxes at low and high levels, respectively, are observed over the equator. Although the PSA2-like wave train shown by HGP at high levels (Figure 4(a)) is still recognizable in the Psi (Figure 4(c)), the negative and positive Psi centres in the central and southern Pacific display a more meridional wave train resembling the first Pacific–South American (PSA1) wave pattern initially described by Karoly (1989). This pattern was also associated with the low-frequency part (40–48 months) of ENSO variability (Mo, 2000). Therefore, the atmospheric circulation at high levels related to the Atuel PC1Ls variability shown in Figure 4 would be a composite manifestation of both the PSA1- and PSA2-like waves associated with the ENSO variability. All these features tend to reverse in the case of water deficit years (i.e. in the −Z1 case).

Regarding the velocity potential (Chi) and the associated non-rotational wind component (Figure 5(c)) near surface ($\sigma = 0.99$, c), correlations indicate air convergence over and adjacent to SA and air divergence on the Drake Passage, associated with the HGP and Psi correlation fields previously described for the Atuel runoff excess (Figure 4). For discharge deficits, these patterns reverse, associated with the strengthening of the Westerlies, south of 40°S, and the semi-permanent anticyclones. At $\sigma = 0.85$ (b) and 0.17 (a), correlation centres reveal opposite convergence and divergence pairs, associated with convection and subsidence anomalies over the eastern and western Pacific respectively for streamflow excesses (vice versa for deficits). Positive (negative) correlations between PC1Ls and PW are recorded in areas where air converges (diverges) and/or northern (southern) flows are observed near surface (see Figures 4 and 5). The band of positive PW correlations extending in NW–SE direction from ~10°S–180°E to ~30°S–80°W is associated with air convergence (Figure 5) and moisture advection from the equatorial Pacific (Figure 4) towards the Atuel basin during high-discharge events.

Above-average discharges in Río Atuel are concurrent with lifting and subsidence air-motion anomalies in the eastern and western Pacific, respectively. These circulation anomalies are coupled with anomalous western and eastern air fluxes respectively at low and high levels over the equatorial Pacific in response to a weakening of the Walker circulation associated with El Niño conditions. These characteristics are reversed for low streamflow years in Rio Atuel (PC1− years) associated with La Niña events. The correlation field between the PCL1s and SST over the tropical Pacific shows the typical pattern associated with El Niño conditions (Figure 6(b)). From Australia to the southern Atlantic, positive (negative) correlations between PC1Ls and air temperatures at 700 hPa (Figure 6(a)) are located west of the anticyclonic (cyclonic) circulation centres with anomalous north (south) winds at 925 hPa. The westward displacement of temperature (T) centres with respect to those of circulation indicates the baroclinic features of these systems. In addition, positive values from ~10°S to 150°W to the South Atlantic through central SA are related to the above-described northwestern circulation at low levels. Between this area and the negative T centres, a strong anomalous T gradient in NW–SE direction is established, which crosses the Atuel basin and reveals an increased baroclinic activity in the area for years of streamflow surplus.

Negative correlations between PC1Ls and SST over the central South Pacific (NE of New Zealand) and the Weddell Sea, in combination with positive correlations on the Amundsen-Bellingshausen Sea, the subtropical South Pacific and the southern coast of Brazil, are related to the above-described air temperature correlation centres at 700 hPa by interactions of momentum and heat transport between the atmosphere and ocean. The circulation is reversed during years with streamflow deficits showing negative temperature anomalies over the Amundsen-Bellingshausen Sea, the subtropical Pacific and Atlantic and the central sector of SA, and positive anomalies east of New Zealand, the South Atlantic and the Weddell Sea. The Walker circulation and the convection over the South Pacific Convergence Zone are strengthened, and SST anomaly patterns correspond to those commonly observed during La Niña events.

Over SA south of 10°S, positive correlations between PC1Ls and surface temperature (T, Figure 4(c)) in northern Chile and Argentina, Paraguay and southern Brazil, reflect the anomalous heat and moisture advections from the subtropical Pacific at low levels. In contrast, negative correlations with T across Patagonia are associated to the advection of polar air from the Weddell Sea (Figures 4 and 6). In addition, positive correlations between PC1Ls and precipitation (PP, Figure 6(d)) are recorded over central Chile, northern and eastern central Patagonia and a large region of southeastern SA. Above-average precipitation in these areas results from an intensification of baroclinic activity due to a northward shift of the storm tracks, an intensification of the advection of heat and moisture from the subtropical Pacific and an attenuation of the Pacific and Atlantic subtropical anticyclones. In particular, the correlation between PC1Ls and PP over Río Atuel basin reaches values of $r > 0.6$. These circulation features are associated with streamflow excess, whereas deficits correspond to opposite atmospheric configurations.

3.2.2. Circulation patterns associated with PC2

Significant spatial correlation patterns between PC2 and climate were identified over two periods within the hydrological cycle: November–December and January. These

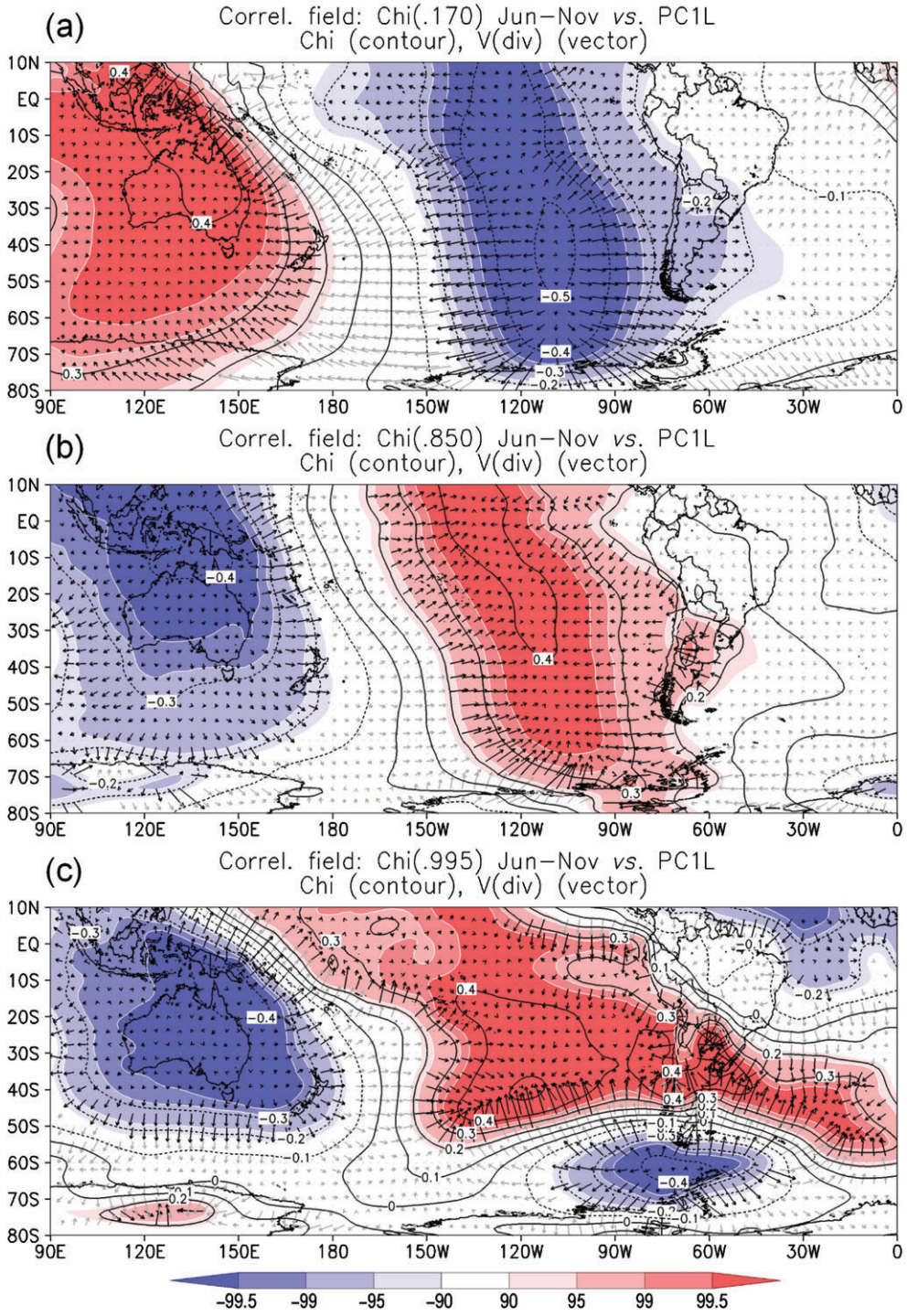

Figure 5. Correlation fields between PC1L and the June–November average for potential velocity at $\sigma = 0.170$ (a), 0.850 (b) and 0.995 (c). Shaded areas from light to dark correspond to significant values at 90, 95, 99 and 99.5% levels (positive in red and negative in blue in online). Vectors represent the non-rotational wind components related to the correlations with potential velocity (in grey for non-significant ones).

patterns are different in each case. Therefore, we assumed that advances or delays of the streamflow in the annual hydrological cycle are induced by atmospheric circulation anomalies occurring in late spring (November–December or December) and summer (January). PC2 correlation fields maximize in November–December or December depending on the persistence and spatial domain (scale) of atmospheric–oceanic variables.

In contrast to the PC1 pattern related to climate variations during a single period (June to November) within the hydrological cycle, the PC2 pattern is related to two periods in the annual cycle. Advances of the annual streamflow peak result from proportionally larger contributions of November and December to the river discharge. However, reductions in streamflow during the following months (particularly January and February), relatively increase the

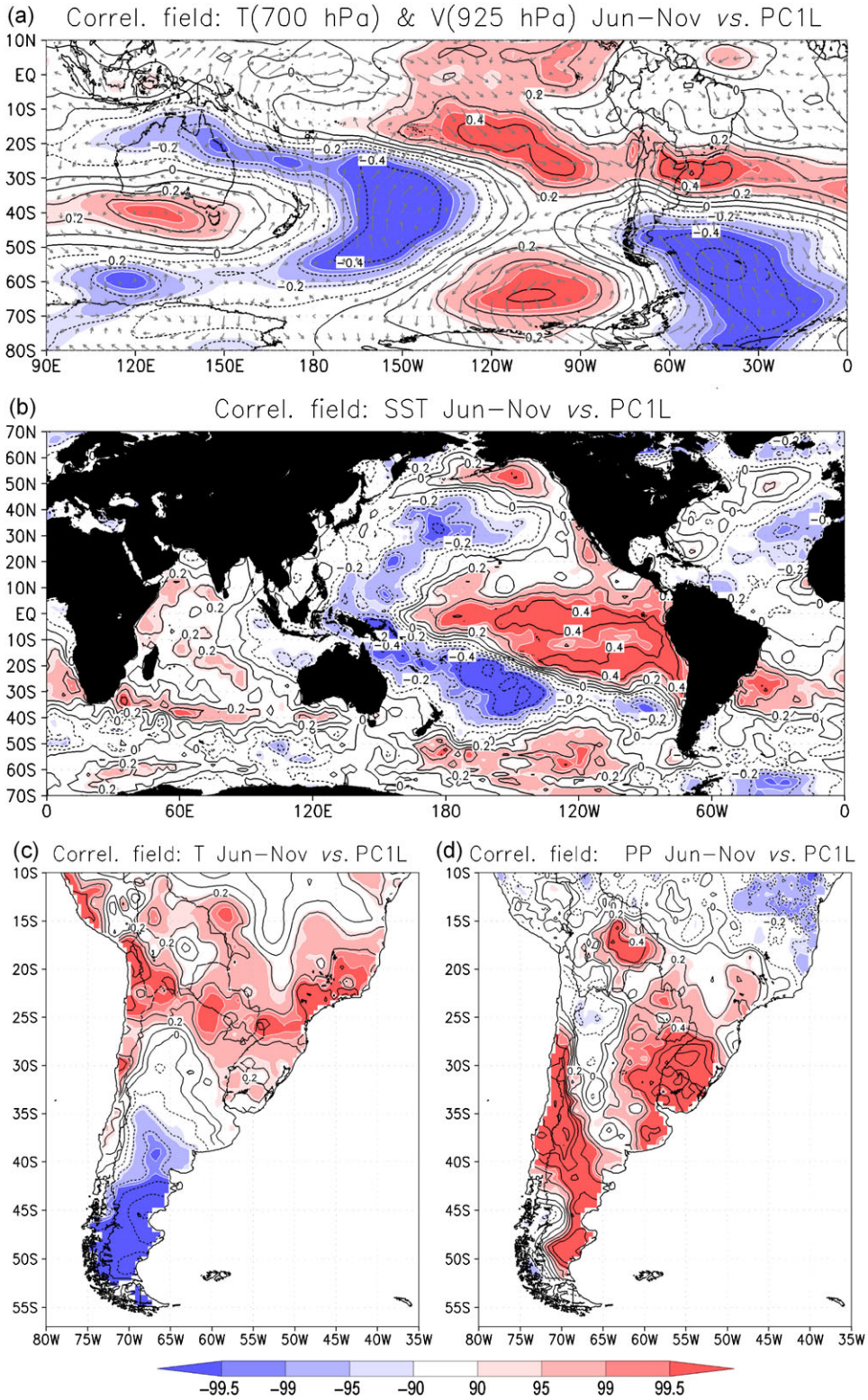

Figure 6. Correlation fields between PC1L and the June–November average for temperature at 700 hPa and wind at 925 hPa (a), sea-surface temperature (b), land-surface temperature (c) and precipitation (d). Shaded areas, from light to dark, correspond to significant values at 90, 95, 99, and 99.5% levels (positive in red and negative in blue in online).

contribution of November–December, although the runoff during November–December is close to normal conditions. Consequently, advances or delays of the annual peak of the water cycle depend on circulation anomalies in both November–December and/or January.

3.2.2.1. Correlation fields in November–December.: Figure 7 (left panels) shows the correlation fields between PC2 and HGP at 500 (a) and 925 hPa (b) levels. At high and low levels in the atmosphere, negative and positive correlations occur south and north of ~60°S,

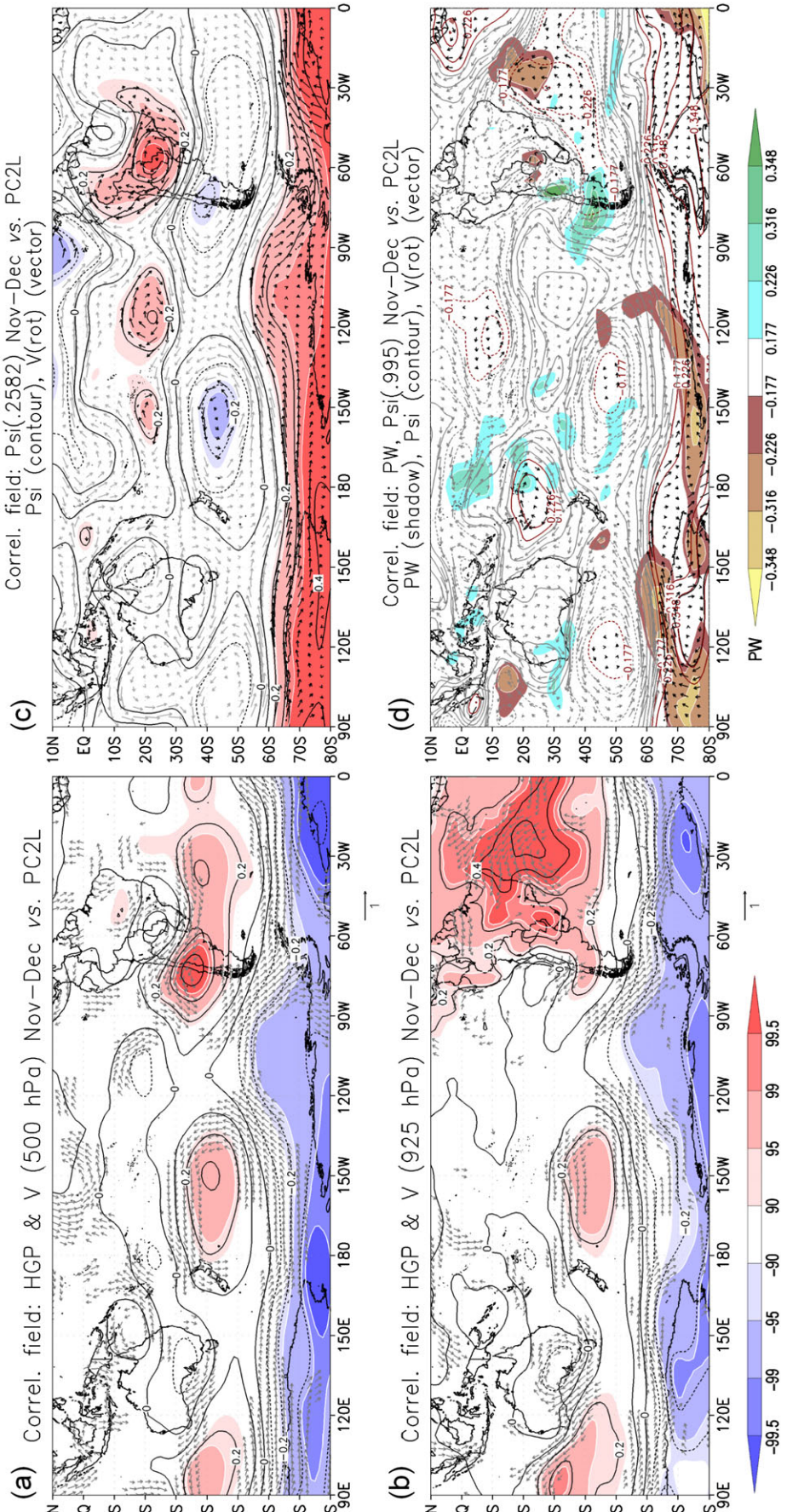

Figure 7. Correlation fields between PC2L and atmospheric circulation variables. Left panels: Correlation fields between PC2L and November–December atmospheric variable means for wind and geopotential height at 500 (a) and 925 hPa (b). Shaded areas, from light to dark, correspond to significant values at 90, 95, 99 and 99.5% levels (positive in red and negative in blue in online). For wind correlation vectors, only those with at least one significant component – u or v – at the 95% level are included. Right panels: as in left panels but for streamfunction at $\sigma = 0.2582$ (c) and for streamfunction at $\sigma = 0.995$ and precipitable water (d). In panel (d), the significant values at 90, 95, 99 and 99.5% levels are indicated by shaded areas for the precipitable water and by dark lines (red in online) for the streamfunction. In both panels (c) and (d), vectors represent the non-divergent circulations associated with the correlations with the streamfunction (in grey for non-significant ones).

respectively. These atmospheric anomalies are associated with a horizontal reinforcement of the pressure gradient and the concurrent intensification of the Westerlies at 50°–60°S latitudes. At the 500-hPa level, the largest positive correlations are recorded between 30°S and 50°S, with maxima over the Indian Ocean, the South Pacific east of New Zealand, the CA of Argentina–Chile and the South Atlantic off the South American coast. This spatial correlation pattern resembles those related to anomalies of the SAM. The most significant correlations at 500 hPa over the Río Atuel basin reflect abnormal warm winds blowing over the upper river basin from the east. Positive correlations at 925 hPa over the Atlantic Ocean and most of the South American continent north of 50°S, reach a maximum over the subtropical ocean. The intensification of the Atlantic anticyclone over this region generates significant eastern wind anomalies on Rio Atuel basin.

Consistent with these circulation patterns, correlations between PC2Ls and the stream function at $\sigma = 0.26$ (Figure 7(c)) show significant positive and negative centres over continental SA, which generates anomalous cyclonic and anticyclonic circulations over central SA and central-south of Chile, respectively, and stronger eastern winds over Río Atuel basin. The anomalous intensification of the Atlantic anticyclone at low levels ($\sigma = 0.995$) induces airflows over Río Atuel basin coming from eastern and central SA and on the eastern slopes of the Andes (Figure 7(d)). This flow intensifies the South American low-level jet and the anomalous transport of heat and moisture from subtropical regions to the Río Atuel basin. The supply of moisture from central Brazil and the Atlantic Ocean is associated with abundant PW over the Atuel region and northern Patagonia. The transport of heat and humidity over the river basin during November–December principally enhances the snow melting and secondarily the occurrence of rainfall, processes that increase the Río Atuel streamflows in these months. The sensible heat released during rainfall also contributes to local temperature increases and snow melt. This warming of the river basin is also reflected by the positive correlations between PC2Ls and T at 700 hPa (Figure 8(a)), which in turn is related to the abnormal increase of HGP at high levels (Figure 7(a)).

Over the Atlantic Ocean, correlations between PC2Ls and SST (Figure 8(b)) show negative and positive values south of the Equator and over the SE coast of SA, respectively. These anomalies respond to the abnormal air fluxes with SE and NE components in the lower layers of the stronger Atlantic anticyclone (Figure 7(b) and (d). The relatively warmer sea off the South American coast increases the heat and humidity carried to the Atuel basin by the eastern air masses.

Locally the abnormal increased temperature and humidity in the basin is confirmed by the correlations between PC2Ls with December temperature and precipitation (Figure 8(c) and (d)). Positive temperature correlations extend over 30°–40°S across SA with maximum values over the Río Atuel basin and northern Patagonia, which are also probably related to the increased pressure represented by the positive correlations of HGP at 500 hPa in the region (Figure 7(a)). Over central SA, weaker significant negative correlations are probably associated with the anomalous trough in the area. Consistent with the advection of subtropical moisture in the region (Figure 7(d)), significant positive correlations with precipitation are observed on the eastern slope of the Andes (Figure 8(d)). However, the contribution of November–December rains to the Río Atuel streamflow is negligible. The snow melting induced by warmer temperatures in these months is comparatively a more important forcing of runoff. The instability caused by the presence of a trough over Paraguay in addition to the increased moisture advection by the low-level jet, intensifies rainfall over central Brazil and the South Atlantic Convergence Zone.

Years with negative PC2Ls are associated with reverse configurations to those described above. The westerly circulation at mid-latitudes, the Atlantic anticyclone and the low-level jet weaken. The enhancement of a high-level cold trough and the strengthening of the western air flow over the Atuel basin region inhibit the transport of heat and moisture from the east, reducing snowmelt and water supply, and consequently the Río Atuel streamflow in November–December.

3.2.2.2. Correlation fields in January: Figure 9 shows the correlation fields between PC2Ls and HGP at 500 (a) and 925 hPa (b) levels. A wave train at 500 hPa consisting of positive-correlation centres over the Tasman Sea, south-central Pacific and the southeast coast of Brazil, is complemented with negative centres over southeastern Australia, south-central Pacific and southern SA. The centres over the central Pacific and the Tasman Sea are at similar locations at low levels, reflecting their barotropic structures. These centres are also shown in the correlation fields with the stream function at $\sigma = 0.995$ (c), representing anomalous anticyclonic circulation over the Tasman Sea and the Pacific at 50°S–110°W and cyclonic circulation at 45°S–160°W. Positive (negative) correlation centres of PW occur with anomalous northern (southern) winds. At the southern tip of SA, anomalous cold and dry air fluxes from the Drake Passage induce the drying of the region and the occurrence of negative correlations with PW near the Río Atuel basin.

Figure 10 shows the correlation fields between PC2Ls and air temperatures at 700 hPa and winds at 925 hPa (a). Positive (negative) centres in the temperature fields coincide with HGP anomalies at 500 hPa and anticyclonic (cyclonic) circulations at low levels, an indication of the barotropic structure of these circulation systems. As part of the hemispheric wave train shown in Figure 9(a), the anomalous cold trough over southern SA favours the persistence of negative T anomalies over most of Argentina and Chile (Figure 10(b)). The high-level trough is also related to instabilities on its northeastern flank, generating positive precipitation anomalies over central-northeastern Argentina, Uruguay and southern Brazil (Figure 10(c)). Negative temperature anomalies over the Atuel basin in

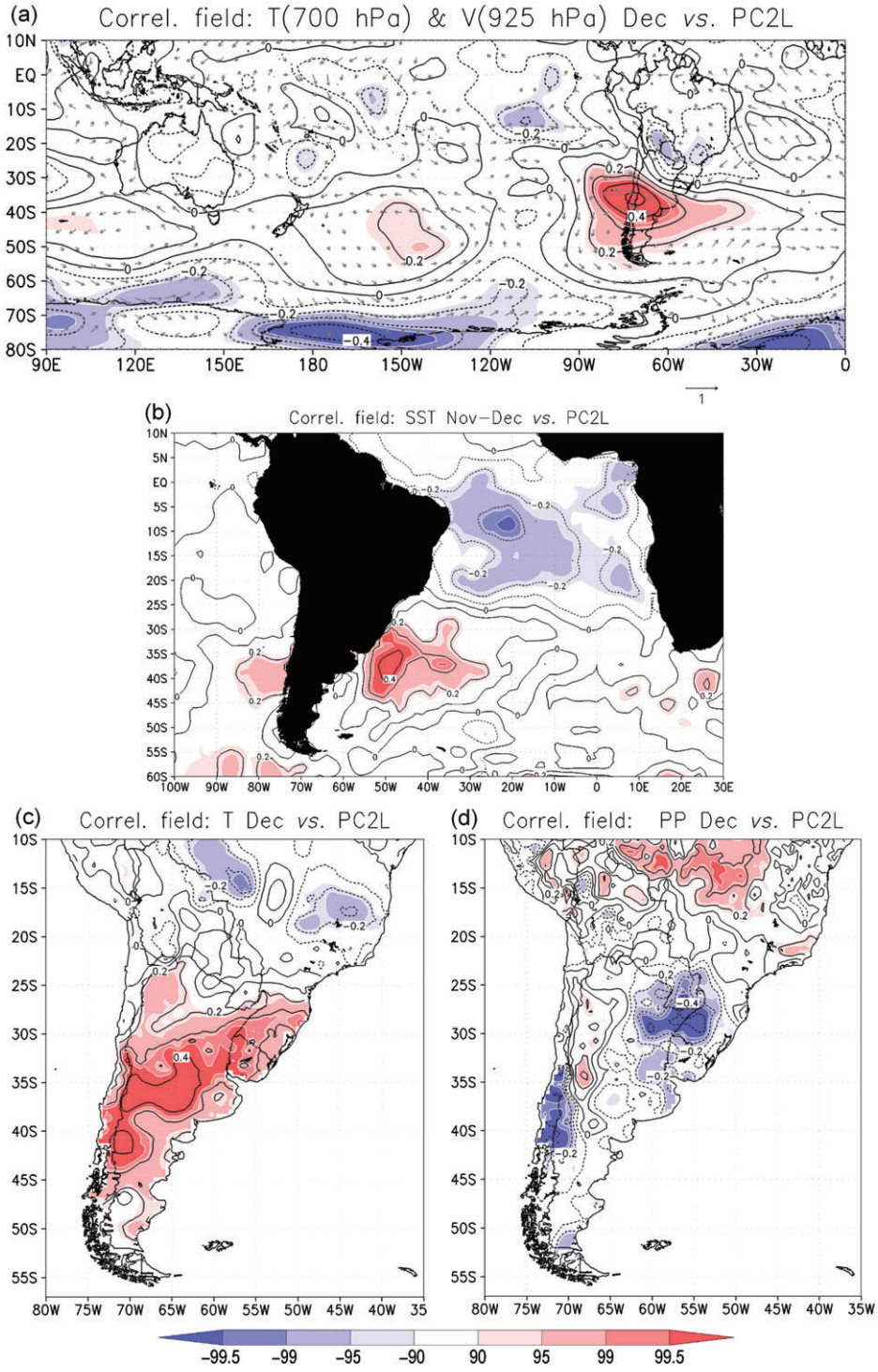

Figure 8. Correlation fields between PC2L and the December atmospheric variable means and the November–December SST means for temperature at 700 hPa and wind at 925 hPa (a), sea-surface temperature (b), land-surface temperature (c) and precipitation (d). Shaded areas, from light to dark, correspond to significant values at 90, 95, 99, and 99.5% levels (positive in red and negative in blue in online).

January inhibit the snowmelt in the upper river basin and the consequent reduction in streamflow.

3.2.3. Composite fields associated with positive and negative PC factor loadings

The time series from PCL in Figure 3(a) and (b) shows decadal to multidecadal periods of mostly positive and negative loadings for both PC1 and PC2 patterns. In order to determine the differences in atmospheric–oceanic conditions associated with the direct and inverse patterns of streamflow cycles, we elaborated spatial composite fields for years with positive (>0.2) and negative (<−0.2) PCL factor loadings.

Figure 11(a) and (b) shows the circulation patterns associated with composite fields for the periods 1977–1987

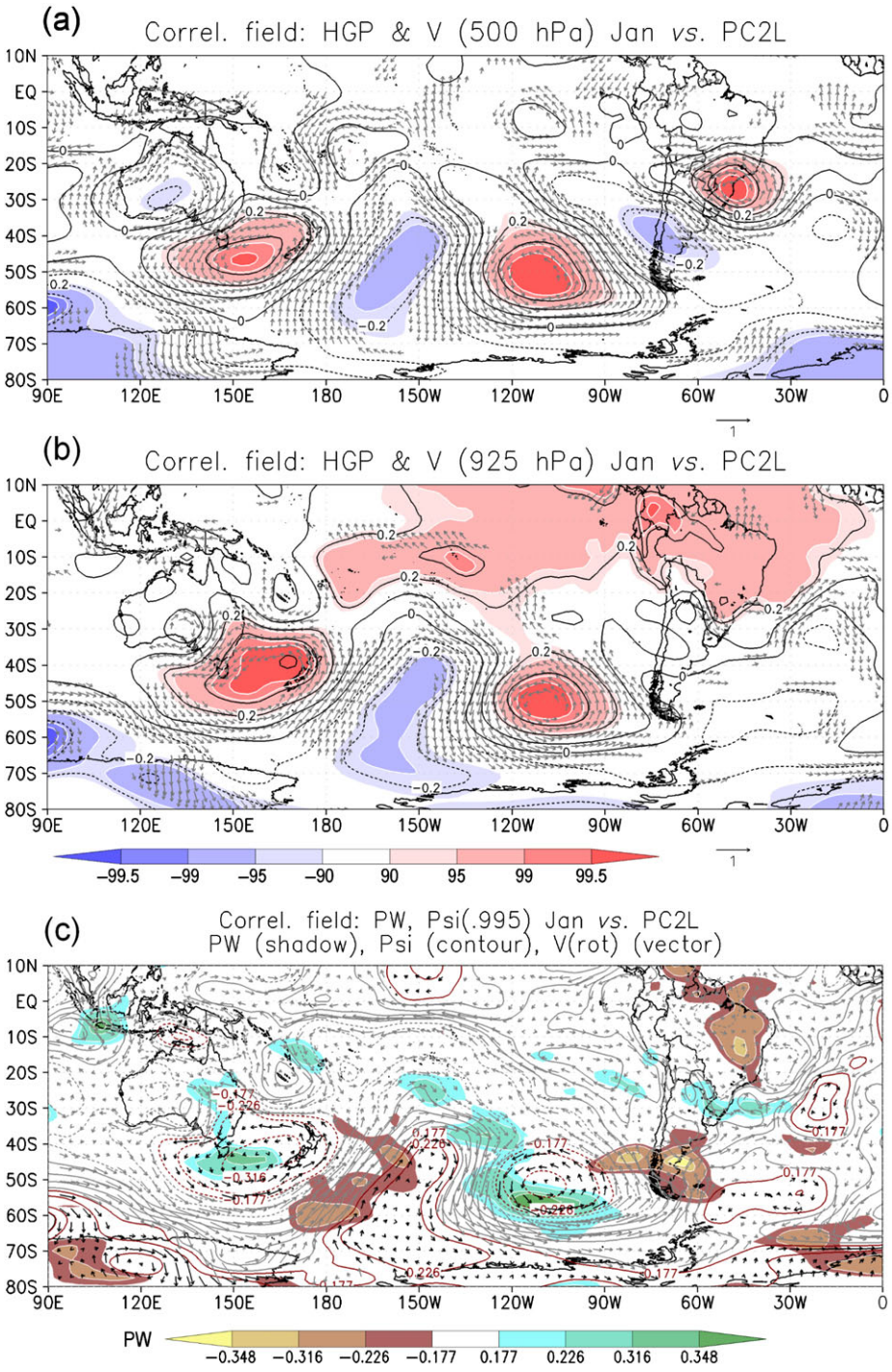

Figure 9. Correlation fields between PC2L and January means of wind and geopotential height at 500 hPa (a) and 925 hPa (b), and of streamfunction at $\sigma = 0.995$ and precipitable water (c). Field characteristics are the same as in Figure 4.

and 1988–2011, characterized by dominant positive and negative PC1Ls, respectively. Positive loadings during the interval 1977–1987 are related to negative and positive HGP anomalies at 850 hPa over the central South Pacific west of SA and southern South Pacific west of the Drake Passage, respectively. These features involve the anomalous intensification of west to north-west winds, increasing the incursion of wet air masses from the tropical South Pacific into the Andes at the latitude of the Río Atuel and the weakening of Westerlies between 40°S and 55°S. Conversely, the composite for the period 1988–2011 dominated by negative PC1Ls, shows positive and negative HGP anomalies across the central South Pacific-SA and west of the Drake Passage-southern South Pacific, respectively, which induces the intensification of the Westerlies at about 50°S and inhibits the arrival of moist air masses to the Río Atuel basin.

There is not a clear distinction of decade-scale periods of persistent positive and negative factors in PC2L over the NCEP reanalysis reference period (Figure 3(b));

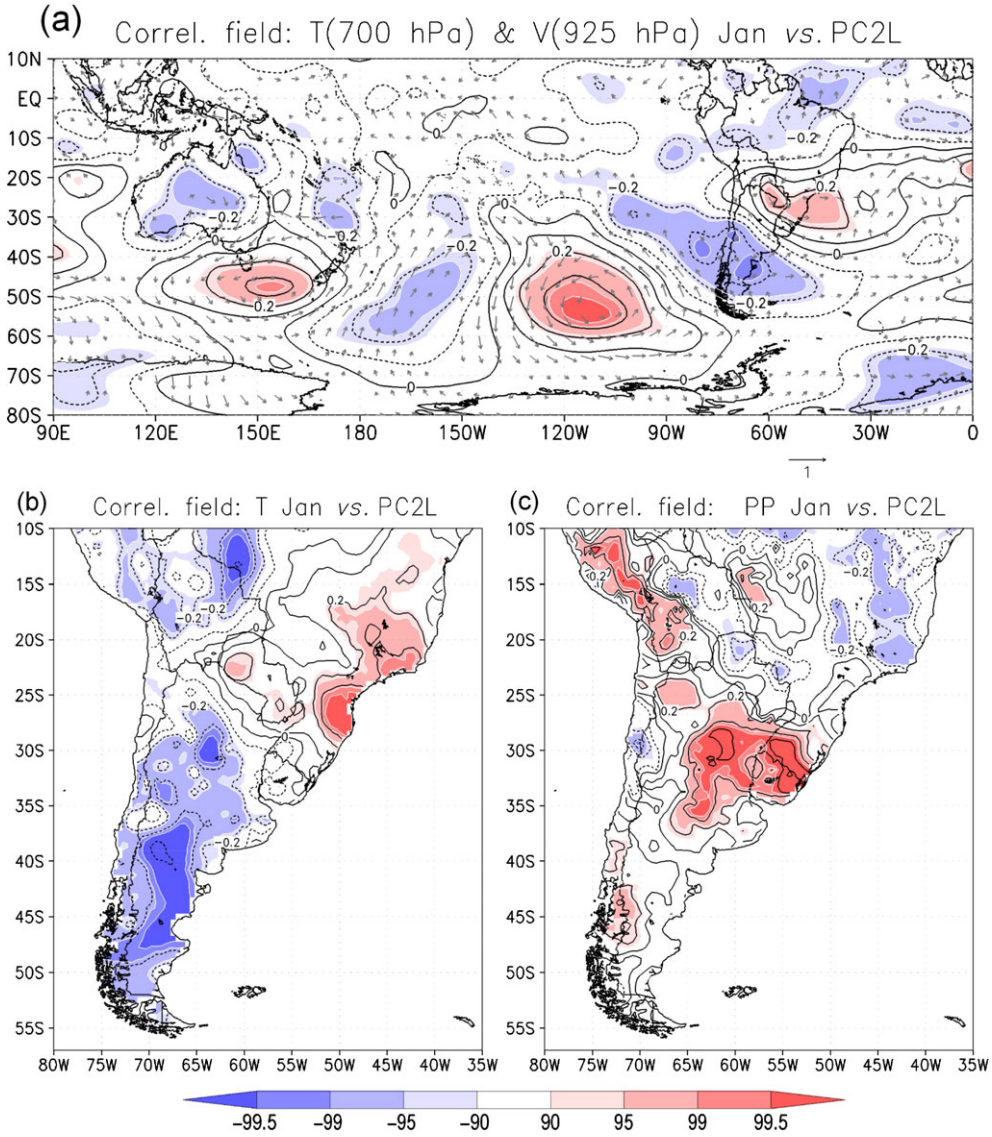

Figure 10. Correlation fields between PC2L and the January atmospheric variables means for temperature at 700 hPa and wind at 925 hPa (a), sea-surface temperature (b), land-surface temperature (c) and precipitation (d). Shaded areas, from light to dark, correspond to significant values at 90, 95, 99, and 99.5% levels (positive in red and negative in blue in online).

therefore, composite fields were estimated using positive (>0.2) and negative (<−0.2) departures in PC2Ls during the whole interval 1958–2012. Composite patterns for HGPs and winds across the Southern Hemisphere clearly show opposite patterns in atmospheric circulation during November–December and January for positive and negative PC2Ls (Figure 11(c) to (f)). For PC2L > 0.2 years, positive (negative) HGP anomalies at 850 hPa are observed north (south) of about 50°–55°S during November–December (Figure 11(c)), with major anomalies over the South Atlantic off the South American coasts. Conversely, for PC2L < −0.2 years, negative (positive) HGP anomalies are observed north (south) of about 55°–60° S (Figure 11(d)). For January, HGP and wind anomalies at 250 hPa for years with PC2L > 0.2 (Figure 11(e)) show a wave train similar to that observed in Figure 9(a), which is in opposite phase for years with PC2L < −0.2 (Figure 11(f)). For other atmospheric–oceanic variables and levels, we also observed consistent similarities between the composites and the correlation fields previously shown.

Table 2 provides a summary of the major patterns in the annual regime of Río Atuel and their relationships with regional and hemispheric atmospheric circulation.

4. Discussion and conclusions

The comprehensive understanding of the hydroclimatic variability in mountainous regions requires long-time series to characterize the whole range of historical variability and trends. The CA of Argentina and Chile are suitable for this type of study given the existence of streamflow series over 100 years in length, including some of the longest in SA. However, interannual variations in river discharges in the CA are extremely large, which

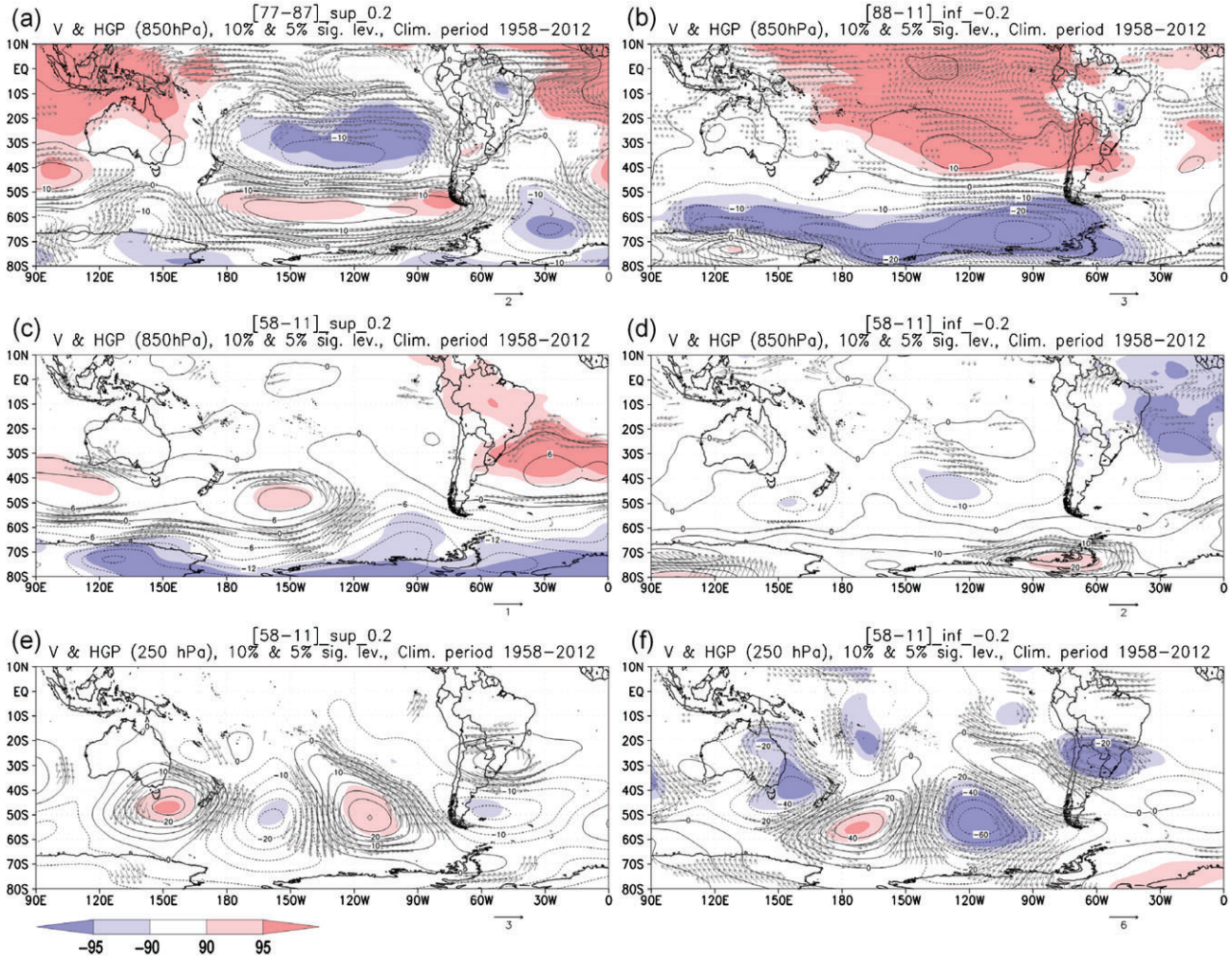

Figure 11. Top panels: Composites of June–November HGP and wind anomalies (based on period 1958–2012) at 850 hPa level for years with PC1L > 0.2 and PC1L < −0.2 during the intervals 1977–1987 (left) and 1988–2011 (right), respectively. Shaded areas, from light to dark, correspond to values at 90 and 95% significant levels (positive in red and negative in blue in online). For wind vectors, only those with at least one significant component – u or v – at the 95% level were included. Middle and bottom panels: As in top panels but for November–December anomalies at 850 hPa level (middle) and for January anomalies at 250 hPa level (bottom); for years with PC2L > 0.2 (left) and PC2L < −0.2 (right) during the interval 1958–2012.

in turn, hamper the proper identification of consistent hydrological trends on a long-term perspective (see Cortés *et al.*, 2011). Year-to-year fluctuations in streamflow over the 20th century, based on ten river records in the CA, vary between 244 (1919) and 38% (1968) of the 1966–2004 reference mean (Masiokas *et al.*, 2010). In this context, we applied PCA to the annual hydrographs of Rio Atuel from 1906 to 2012 to separate the dominant mode of variability related to interannual fluctuations in total streamflow and examine the remaining PCs to identify changes unrelated to year-to-year variability in total runoff. PC1 explains 49% of the total variance in the hydrological cycle and corresponds to the dominant signal in the Río Atuel annual cycle imposed by streamflows above (below) the mean (Figure 2). Therefore, PC1 is largely related to interannual and long-term variability of the total runoff. In contrast, PC2, which represents 21% of the total variance in the hydrological cycle, is associated with seasonal shifts of the monthly streamflow peak occurring late in spring (direct mode) or late in summer (inverse mode; Figure 2). The advance (delay) of the annual peak is modulated by the early (belated) onset of the warm season or a relatively cool summer (spring).

A variety of non-natural causes, such as changes in the river section geometry or systematic measurement errors, may induce spurious changes in runoff. Therefore, to validate the regional representativeness of the results recorded in the analysis of Rio Atuel streamflow, we applied PCA to the annual cycles of Río Mendoza and Río Tunuyán, both basins located in the CA of Argentina. PC1 and PC2 patterns from these rivers are similar to those of Rio Atuel, showing correlation coefficients between PCLs larger than $r = 0.6$ (significant at 99% confidence level). Comparison of these results with patterns from other rivers in the CA indicates that the results presented in this study are representative of the region.

Our results indicated that the variability of the Río Atuel annual cycle can be decomposed into a snow-

Table 2. Summary of main results.

Principal component	Mode	Hydrological regime	Months	Local meteorological conditions		Atmospheric circulation and climatic conditions
				PP anomalies	T anomalies	
PC1	+	Above-mean streamflows	Jun–Nov	+	nr	Positive and negative HGP anomalies west of the Drake Passage and over subtropical South Pacific, respectively. Northward shift of stormtracks remotely induced by positive SST anomalies in the equatorial Pacific (El Niño conditions/positive PDO phase)
	–	Below-mean streamflows		–	nr	Negative and positive HGP anomalies west of the Drake Passage and over subtropical South Pacific, respectively. Southward shift of stormtracks remotely induced by negative SST anomalies in the equatorial Pacific (La Niña conditions/negative PDO phase)
PC2	+	Advanced streamflow peak to late spring	Nov–Dec	nr	+	Strengthening of the South Atlantic anticyclone which in turn enhances the tropical meridional circulation over the Atuel basin (linked to the positive phase of the SAM)
			Jan	nr	–	Anomalous air cooling over the Atuel basin induced by low pressure anomalies at high levels as part of a quasi-zonal stationary Rossby wave train extending from Australia
	–	Belated streamflow peak to late summer	Nov–Dec	nr	–	Weakening of the South Atlantic anticyclone which in turn enhances the sub-Antarctic meridional circulation over the Atuel basin (linked to the negative phase of the SAM)
			Jan	nr	+	Anomalous air warming over the Atuel basin induced by high-pressure anomalies at high levels as part of a quasi-zonal stationary Rossby wave train extending from Australia

nr, not related.

dependent component in winter, which determines the above/below normal runoff variability (PC1), and into a thermal-dependent component of spring–summer, which determines the seasonal shift of the monthly streamflow peak (PC2). Figure 12(a) compares the annual variations in PC1Ls with an index of regional precipitation. Given the lack of meteorological stations with long reliable records in the high mountains, the index was calculated over the interval 1917–2010 as the average of June–November rainfall records, previously standardized over the common period (1951–2010) from Santiago (at Pudahuel), Curicó and Concepción stations in the Central Chile valley (Figure 1). The selection of these weather stations is consistent with the spatial correlation field shown in Figure 6(d) and recent studies by Masiokas *et al.* (2012), who determined a very strong correlation between rainfall in the central valley of Chile and Andean streamflow ($r = 0.88$, $n = 90$ years, period 1909–1998). A significant correlation ($r = 0.66$, $n = 94$, $p < 0.01$) between PC1Ls and the regional precipitation index is consistent with the fact that the amount of snow accumulated in winter in the high mountains is the principal driver of interannual variability in Río Atuel discharge.

Based on the spatial correlation pattern shown in Figure 8(c), we compared interannual variations of PC2Ls with temperature records on the eastern side of the Andes. As variations of spring–summer temperatures in the Rio Atuel basin are largely controlled by atmospheric circulation east of the Andes, temperature records from San Luis, Santa Rosa and San Rafael stations (Figure 1 and Table 1) were used to produce a regional temperature index. For each station, the December minus January temperature differences were standardized by subtracting the mean and dividing by the standard deviation estimated over the common period between the three records. The resulting standardized series were then averaged to obtain the index (Figure 12(b)). For the interval 1960–2009, variations in December minus Jan temperature are significantly correlated with PC2Ls ($r = 0.60$, $n = 50$, $p < 0.01$). Similar levels of statistical significance in the relationships between PC2Ls and temperature were recorded using a temperature index based on a longer season (September to December instead of just December; $r = 0.55$, $n = 50$, $p < 0.01$), suggesting that an earlier centre of mass in the streamflows can also be influenced by warmer temperature prior to December. Correlations between PC1Ls and the temperature

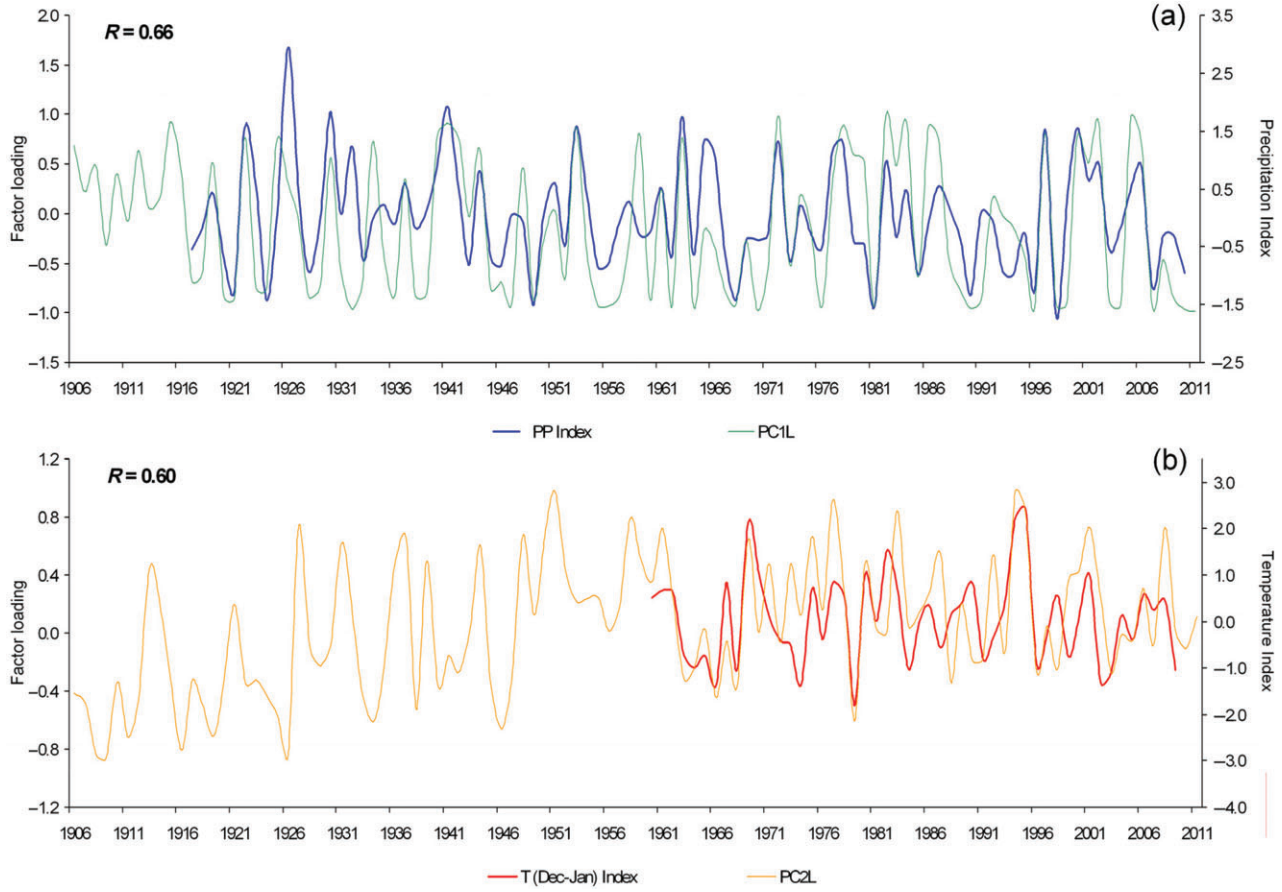

Figure 12. (a) PC1L (green in online) and regional precipitation index (blue in online) over the interval 1916–2011 (see text). (b) PC2L (orange in online) and regional temperature index (red in online) over the interval 1961–2009. Correlation coefficients between series in 1917–2010 (a) and 1960–2009 (b) are given on each panel.

index, and between PC2Ls and winter precipitation, are not significant confirming the dominant influences of precipitation and temperature on PC1Ls and PC2Ls, respectively.

The temporal evolution of the PCLs reveals that the PC1 pattern was predominantly inverse (negative loadings) during the periods 1917–1976 and 1988 to present, which suggests the propensity of the hydrological regimes to undergo extended periods of streamflow deficits. In turn, the PC2 pattern is predominantly inverse from 1906 to 1926 and direct (positive loadings) from 1948 to present, suggesting a pattern change to one with streamflow peaks during late spring in most years since the second half of the 20th century (Figure 3). Our results are consistent with Cortés *et al.* (2011) indicating that warmer springs north of 35°S in the CA favour snowmelt onset and shift flows earlier in the annual cycle.

Our results are also consistent with previous studies indicating that interannual variations in the total streamflow and the timing centre of Río Atuel flows result from changes in climate forcings from synoptic- to global scale (Aceituno and Vidal, 1990; Waylen and Caviedes, 1990; Masiokas *et al.*, 2006). The direct (inverse) PC1 pattern is related to significant positive (negative) pressure anomalies west of the Drake Passage and negative (positive) anomalies over subtropical South Pacific reaching the Río Atuel basin. In addition, warmer (cooler) SST anomalies are observed in the central equatorial Pacific during the direct (inverse) PC1 years. Hence, years with summer streamflows above (below) the normal are related to abundant (reduced) snowfalls in the high CA in response to a northward (southward) shift of the storm-tracks remotely induced by SST anomalies in the equatorial Pacific (El Niño/La Niña events; correlation coefficient between June–November El Niño 3.4 SST and PC1Ls is $r = 0.33$, $n = 106$, $p < 0.01$). Recent studies indicated that long-term changes in the CA streamflows are modulated by the Pacific Decal Oscillation (Masiokas *et al.*, 2010).

As advances in timing of the hydrological peak can be related to warmer November–December or colder January conditions over the CA, differences in atmospheric circulation for both periods are relevant. The propensity to increase (to reduce) the streamflow peak in November–December is related to above-average (below-average) temperatures over the CA, which are induced by the strengthening (weakening) of the South Atlantic anticyclone which in turn enhances the tropical (sub-Antarctic) meridional circulation over Río Atuel latitudes. These circulation anomalies are linked to the positive (negative) phase of the SAM (Silvestri and Vera,

2009; Villalba *et al.*, 2012). Additionally, years with a propensity to reduce (to increase) the streamflow peak in January are associated with anomalous air cooling (warming) at high levels induced by low (high) pressure anomaly centres as part of a quasi-zonal stationary Rossby wave train extending from Australia to the South Atlantic.

Future climate scenarios associated with global warming indicate a decrease in winter precipitation in the CA of Argentina and Chile accompanied by a progressive increase, particularly in summer, of temperatures (IPCC, 2013). Following these scenarios, reductions in streamflows in the CA would be accompanied by progressive advancement in the snowmelt, and consequently, in the occurrence of peak runoff. However, recent studies indicate that persistently positive SAM trends, related to warmer conditions in the Río Atuel basin, have been forced by tropospheric ozone depletion over the Antarctic continent (Polvani *et al.*, 2011; Villalba *et al.*, 2012). It is possible that the tropospheric ozone recovery could reverse the positive trends of the SAM in the coming years and therefore the temperature increases over the CA, with the resulting offset of the advances in the timing of the centre of streamflows.

Acknowledgements

This work was supported by the Argentinean Council of Research and Technology (CONICET) PIP 2010–439 and by the Inter-American Institute for Global Change Research (IAI) CRN 2047, which is supported by the US National Science Foundation (Grant GEO-0452325).

References

Aceituno P. 1988. On the functioning of the southern oscillation in the South American Sector. I: Surface climate. *Mon. Weather Rev.* **116**: 505–524.

Aceituno P, Garreaud R. 1995. Impactos de los fenómenos El Niño y La Niña sobre regímenes fluviométricos andinos. *Rev. Soc. Chilena de Ing. Hidráulica* **10**(2): 33–43.

Aceituno P, Vidal F. 1990. Variabilidad interanual en el caudal de ríos andinos en Chile Central en relación con la temperatura de la superficie del mar en el Pacífico Central. *Rev. Soc. Chilena de Ing. Hidráulica* **5**(1): 7–19.

Araneo DC, Compagnucci RH. 2008. Atmospheric circulation features associated to Argentinean Andean rivers discharge variability. *Geophys. Res. Lett.* **35**(1): 1–6, doi: 10.1029/2007GL032427.

Barnett TP, Pierce DW, Hidalgo HG, Bonfils C, Santer BD, Das T, Bala G, Wood AW, Nozawa T, Mirin AA, Cayan DR, Dettinger MD. 2008. Human-induced changes in the hydrology of the western United States. *Science* **319**: 1080–1083.

Carrasco JF, Casassa G, Quintana J. 2005. Changes of the 0°C isotherm and the equilibrium line altitude in central Chile during the last quarter of the 20th century. *Hydrol. Sci. J.* **50**: 933–948.

Cayan DR, Dettinger MD, Diaz HF, Graham NE. 1998. Decadal variability of precipitation over western North America. *J. Clim.* **11**: 3148–3166.

Clow DW. 2010. Changes in the timing of snowmelt and streamflow in Colorado: a response to recent warming. *J. Clim.* **23**(9): 2293–2306, doi: 10.1175/2009JCLI2951.1.

Compagnucci RH, Araneo DC. 2005. Identificación de áreas de homogeneidad estadística para los caudales de ríos andinos argentinos y su relación con la circulación atmosférica y la temperatura superficial del mar. *Meteorologica* **30**(1, 2): 41–53.

Compagnucci R, Araneo D. 2007. Alcances de El Niño como predictor del caudal de los ríos andinos argentinos. *Ing. Hidrául. Méx.* **22**(3): 23–35.

Compagnucci RH, Vargas W. 1998. Interannual variability of Cuyo Rivers streamflow in Argentinean Andean Mountains and ENSO events. *Int. J. Climatol.* **18**: 1593–1609.

Cortés G, Vargas X, McPhee J. 2011. Climatic sensitivity of streamflow timing in the extratropical western Andes Cordillera. *J. Hydrol.* **405**(1–2): 93–109, doi: 10.1016/j.jhydrol.2011.05.013.

Dettinger MD, Cayan DR, Meyer MK, Jeton AE. 2004. Simulated hydrologic responses to climate variations and change in the Merced, Carson, and American River basins, Sierra Nevada, California, 1900–2099. *Clim. Chang.* **62**: 283–317.

Escobar F, Aceituno P. 1998. Influencia del fenómeno ENSO sobre la precipitación nival en el sector andino de Chile central durante el invierno. *Bull. Inst. Fr. Études Andin.* **27**(3): 753–759.

Falvey M, Garreaud RD. 2009. Regional cooling in a warming world: recent temperature trends in the southeast Pacific and along the west coast of subtropical South America (1979–2006). *J. Geophys. Res.* **114**: D04102, doi: 10.1029/2008JD010519.

Hamlet AF, Mote PW, Clark MP, Lettenmaier DP. 2007. Twentieth-century trends in runoff, evapotranspiration, and soil moisture in the western United States. *J. Clim.* **20**: 1468–1486.

Hoffman JA. 1969. *Pronóstico Del Tiempo a Largo Plazo (2da. Parte)*. Primeras Jornadas de Nivo-Glaciología, Fac. Cs. Pol. y Soc. UNC: Mendoza, Argentina.

IPCC. 2013. Climate Change 2013: The Physical Science Basis. *Contribution of Working Group I to the Fifth Assessment Report of the Intergovernmental Panel on Climate Change*, Stocker TF, Qin D, Plattner G-K, Tignor M, Allen SK, Boschung J, Nauels A, Xia Y, Bex V, Midgley PM (eds). Cambridge University Press: Cambridge, UK and New York, NY, 1535 pp.

Kalnay E et al. 1996. The NCEP/NCAR 40-year reanalysis project. *Bull. Am. Meteorol. Soc.* **77**: 437–470.

Karoly DJ. 1989. Southern Hemisphere circulation features associated with El Niño–Southern Oscillation events. *J. Clim.* **2**: 1239–1251.

Knowles N, Cayan DR. 2004. Elevational dependence of projected hydrologic changes in the San Francisco Estuary and watershed. *Clim. Chang.* **62**: 319–336.

Masiokas MH, Villalba R, Luckman BH, Le Quesne C, Aravena JC. 2006. Snowpack variations in the central Andes of Argentina and Chile, 1951–2005: large-scale atmospheric influences and implications for water resources in the Region. *J. Clim.* **19**: 6334–6352.

Masiokas MH, Luckman BH, Villalba R, Delgado S, Rabassa J. 2010. Little Ice Age fluctuations of Glaciar Río Manso in the north Patagonian Andes of Argentina. *Quaternary Res.* **73**: 96–106.

Masiokas MH, Villalba R, Christie DA, Betman E, Luckman BH, Le Quesne C, Prieto MR, Mauget S. 2012. Snowpack variations since AD 1150 in the Andes of Chile and Argentina (30°-37°S) inferred from rainfall, tree-ring and documentary records. *J. Geophys. Res.* **117**: 1–11.

Minetti JL, Sierra EM. 1989. The influence of general circulation patterns on humid and dry years in the Cuyo Andean region of Argentina. *Int. J. Climatol.* **9**(1): 55–68, doi: 10.1002/joc.3370090105.

Mo K. 2000. Relationships between low-frequency variability in the Southern Hemisphere and sea surface temperature anomalies. *J. Clim.* **13**: 3599–3610.

Montecinos A, Aceituno P. 2003. Seasonality of the ENSO related rainfall variability in central Chile and associated atmospheric circulation. *J. Clim.* **16**: 281–296.

Mote PW, Hamlet AF, Clark MP, Lettenmaier DP. 2005. Declining mountain snowpack in western North America. *Bull. Am. Meteorol. Soc.* **86**: 39–49.

Pierce DW, Barnett TP, Hidalgo HG, Das T, Bonfils C, Santer BD, Bala G, Dettinger MD, Cayan DR, Mirin A, Wood AW, Nozawa T. 2008. Attribution of declining Western U.S. snowpack to human effects. *J. Clim.* **21**(23): 6425–6444, doi: 10.1175/2008JCLI2405.1.

Pittock AB. 1980. Patterns of climatic variation in Argentina and Chile. Part I: Precipitation, 1931–1960. *Mon. Weather Rev.* **108**: 1347–1361.

Polvani LM, Waugh DW, Correa GJP, Son S-W. 2011. Stratospheric ozone depletion: the main driver of 20th century atmospheric circulation changes in the Southern Hemisphere. *J. Clim.* **24**: 795–812.

Prohaska F. 1976. The climate of Argentina, Paraguay and Uruguay. In *World Survey of Climatology*, Vol. 12, Schwerdtfeger W (ed). Elsevier: Amsterdam, 13–112.

Quinn W, Neal V. 1983. Long-term variations in the Southern Oscillation, El Niño and the Chilean subtropical rainfall. *Fish. Bull.* **81**: 363–374.

Regonda SK, Rajagoplan B, Clark M, Pitlick J. 2005. Seasonal cycle shifts in hydroclimatology over the western United States. *J. Clim.* **18**: 372–384.

Rodionov SN. 2004. A sequential algorithm for testing climate regime shifts. *Geophys. Res. Lett.* **31**(9): L09204, doi: 10.1029/2004GL019448.

Rutllant J. 1987. Synoptic aspects of the increase in rainfall in Central Chile associated with warm events in the Central Equatorial Pacific. *Proceedings of the Conference on Geophysical Fluid Dynamics with Special Emphasis on El Niño.* Sao Jose dos Campos, 13–17 July 1987, 329–342.

Rutllant J, Fuenzalida H. 1991. Synoptic aspects of the central Chile rainfall variability associated with the Southern Oscillation. *Int. J. Climatol* **11**: 63–76.

Schwerdtfeger W. 1976. High thunderstorm frequency over the subtropical Andes during summer: cause and effects. In *Climate of Central and South America*, Schwerdtfeger W (ed). Elsevier: Amsterdam, 192–195.

Silvestri G, Vera C. 2009. Nonstationary impacts of the southern annular mode on Southern Hemisphere climate. *J. Clim.* **22**(22): 6142–6148, doi: 10.1175/2009JCLI3036.1.

Stewart IT, Cayan DR, Dettinger MD. 2005. Changes toward earlier streamflow timing across western North America. *J. Clim.* **18**: 1136–1155.

Thompson DWJ, Wallace JM. 2000. Annular modes in the extratropical circulation. Part I: Month-to-month variability. *J. Clim.* **13**: 1000–1016.

Villalba R, Lara A, Masiokas MH, Urrutia R, Luckman BH, Marshall GJ, Mundo IA, Christie DA, Cook ER, Neukom R, Allen K, Fenwick P, Boninsegna JA, Srur AM, Morales MS, Araneo D, Palmer JG, Cuq E, Aravena JC, Holz A, Le Quesne C. 2012. Unusual Southern Hemisphere tree growth patterns induced by changes in the Southern Annular Mode. *Nat. Geosci.* **5**(11): 793–798, doi: 10.1038/ngeo1613.

Waylen P, Caviedes C. 1990. Annual and seasonal fluctuations of precipitation and stream flow in the Aconcagua river basin, Chile. *J. Hydrol.* **120**: 79–102.

